Functional characterization of cytochrome P450-derived epoxyeicosatrienoic acids in adipogenesis and obesity

Weibin Zha,* Matthew L. Edin,† Kimberly C. Vendrov,* Robert N. Schuck,* Fred B. Lih,† Jawahar Lal Jat,§ J. Alyce Bradbury,† Laura M. DeGraff,† Kunjie Hua, Kenneth B. Tomer,† John R. Falck,§ Darryl C. Zeldin,† and Craig R. Lee[1,*]**

Division of Pharmacotherapy and Experimental Therapeutics, Eshelman School of Pharmacy,*and UNC Nutrition Obesity Research Center,** University of North Carolina, Chapel Hill, NC; Laboratory of Respiratory Biology,† Division of Intramural Research, National Institute of Environmental Health Sciences, National Institutes of Health, Research Triangle Park, NC; and Department of Biochemistry,§ University of Texas Southwestern Medical Center, Dallas, TX

Abstract Adipogenesis plays a critical role in the initiation and progression of obesity. Although cytochrome P450 (CYP)-derived epoxyeicosatrienoic acids (EETs) have emerged as a potential therapeutic target for cardiometabolic disease, the functional contribution of EETs to adipogenesis and the pathogenesis of obesity remain poorly understood. Our studies demonstrated that induction of adipogenesis in differentiated 3T3-L1 cells (in vitro) and obesity-associated adipose expansion in high-fat diet (HFD)-fed mice (in vivo) significantly dysregulate the CYP epoxygenase pathway and evoke a marked suppression of adipose-derived EET levels. Subsequent in vitro experiments demonstrated that exogenous EET analog administration elicits potent anti-adipogenic effects via inhibition of the early phase of adipogenesis. Furthermore, EET analog administration to mice significantly mitigated HFD-induced weight gain, adipose tissue expansion, pro-adipogenic gene expression, and glucose intolerance. Collectively, these findings suggest that suppression of EET bioavailability in adipose tissue is a key pathological consequence of obesity, and strategies that promote the protective effects of EETs in adipose tissue offer enormous therapeutic potential for obesity and its downstream pathological consequences.—Zha, W., M. L. Edin, K. C. Vendrov, R. N. Schuck, F. B. Lih, J. L. Jat, J. A. Bradbury, L. M. DeGraff, K. Hua, K. B. Tomer. J. R. Falck, D. C. Zeldin, and C. R. Lee. **Functional characterization of cytochrome P450-derived epoxyeicosatrienoic acids in adipogenesis and obesity. *J. Lipid Res.* 2014.** 55: **2124–2136.**

Supplementary key words adipose tissue • arachidonic acid • eicosanoids • high-fat diet • metabolomics • soluble epoxide hydrolase

Obesity is a major public health problem that contributes to the development of type 2 diabetes and cardiovascular disease (1). Excessive lipid accumulation in adipose tissue is a key pathological driver of obesity, and is manifested by an increase in the number (hyperplasia) and size (hypertrophy) of adipocytes. Differentiation of preadipocytes to mature adipocytes (adipogenesis) is an integral mediator of this process, and is under the control of a transcription factor network that regulates lipid biosynthesis and metabolism (2). Most notably, PPAR-γ, CCAAT/enhancer-binding protein (C/EBP)α, and sterol regulatory-element-binding protein (SREBP)1c are central mediators of this process through the regulation of LPL, acetyl-CoA carboxylase 1 (ACC1), and FAS expression (2, 3). Sustained activation of this process, however, is a key pathological driver of obesity that results in adipocyte dysfunction, glucose intolerance, and ultimately the development of insulin resistance and type 2 diabetes (4, 5). Consequently, an improved understanding of the key pathways that regulate adipogenesis and adipocyte function offers enormous potential to facilitate the development of novel therapeutic strategies that mitigate the development and progression of obesity-associated metabolic diseases.

This work was supported by grant R01 GM088199 to C.R.L.; a predoctoral fellowship from the American Heart Association to R.N.S.; grant GM31278 and support from the Robert A. Welch Foundation to J.R.F.; grant P30 DK34987 to the UNC Center for Gastrointestinal Biology and Disease; grant P30 DK056350 to the UNC Nutrition Obesity Research Center; and funds from the Intramural Research Program of the National Institutes of Health, National Institute of Environmental Health Sciences to K.B.T. (Z01 ES050167) and D.C.Z. (Z01 ES025034).

Manuscript received 18 July 2014.

Published, JLR Papers in Press, August 11, 2014
DOI 10.1194/jlr.M053199

Abbreviations: ACC1, acetyl-CoA carboxylase 1; AMPK, AMP-activated protein kinase; AUC, area under the concentration-time curve; BAT, brown adipose tissue; C/EBP, CCAAT/enhancer-binding protein; CYP, cytochrome P450; DHET, dihydroxyeicosatrienoic acid; EET, epoxyeicosatrienoic acid; EET-A, (S)-2-(13-(3-butylureido) tridec-8(Z)-enamido)succinic acid; eWAT, epididymal white adipose tissue; Fabp4, fatty acid binding protein 4; FDR, false discovery rate; H&E, hematoxylinandeosin;HFD,high-fatdiet;MS-PPOH,N-(methylsulfonyl)-2-(2-propynyloxy)-benzenehexanamide; NIH, National Institutes of Health; NUDSA, (S)-2-(11-(nonyloxy) undec-8(Z)-enamido)succinic acid; PCA, principal components analysis; qRT-PCR, quantitative RT-PCR; RER, respiratory exchange ratio; SREBP, sterol regulatory-element-binding protein; sEH, soluble epoxide hydrolase; UCP1, uncoupling protein 1; VHFD, very high-fat diet; VO_2, oxygen consumption; VCO_2, carbon dioxide production.

[1]To whom correspondence should be addressed.
e-mail: craig_lee@unc.edu

In addition to a well-established role in xenobiotic metabolism, cytochromes P450 (CYPs) metabolize essential fatty acids to bioactive eicosanoids in various cell types. Most notably, arachidonic acid is metabolized by CYP2J and CYP2C epoxygenases to epoxyeicosatrienoic acids (EETs), which are rapidly hydrolyzed by soluble epoxide hydrolase (sEH, *Ephx2*) (6). CYP-derived EETs are key regulators of a myriad of biological processes in the cardiovascular system, including vascular tone and inflammation (7, 8). It also has been reported that EETs elicit protective effects in obesity-associated metabolic disease (9–12). However, the impact of adipogenesis and obesity on EET biosynthesis in adipose tissue and the functional role of EETs in the regulation of adipogenesis and the pathogenesis of obesity remains poorly understood.

Consequently, using established in vitro (differentiated 3T3-L1 cells) and in vivo [high-fat diet (HFD)-fed mice] models, we investigated: *a*) the impact of adipogenesis and obesity on the bioavailability of adipose-derived EETs; and *b*) the functional effects of EETs on adipogenesis and obesity, and their downstream pathological consequences.

MATERIALS AND METHODS

Reagents

Reagents were obtained from Sigma-Aldrich (St. Louis, MO) unless otherwise indicated. The stable EET analog 14,15-epoxyeicosa-8(Z)-enoic acid (14,15-EE-8(Z)-E) and CYP epoxygenase inhibitor N-(methylsulfonyl)-2-(2-propynyloxy)-benzenehexanamide (MS-PPOH) were purchased from Cayman Chemical (Ann Arbor, MI). The stable EET analogs (S)-2-(11-(nonyloxy) undec-8(Z)-enamido)succinic acid (NUDSA) and (S)-2-(13-(3-butylureido) tridec-8(Z)-enamido)succinic acid (EET-A, sodium salt) were synthesized by Dr. John Falck (University of Texas Southwestern, TX) (13, 14).

Peptide-based antibodies that cross-react with murine Cyp2c55 (anti-Cyp2c55 #1545) and Cyp2j9 (anti-Cyp2j9pep2), and recombinant Cyp2c55 and Cyp2j9 proteins, were provided by Dr. Darryl Zeldin (National Institute of Environmental Health Sciences, Research Triangle Park, NC) (15, 16). Antibodies against murine sEH (sc22344) and GAPDH (#2118) were purchased from Santa Cruz Biotechnology (Santa Cruz, CA) and Cell Signaling Technology (Danvers, MA), respectively.

3T3-L1 cell culture and differentiation

Murine 3T3-L1 preadipocytes were obtained from ATCC (Manassas, VA). Preadipocytes were cultured to confluence in DMEM with 10% newborn calf serum and 1% penicillin-streptomycin at 37°C with 5% CO_2, and then chemically differentiated into mature adipocytes over 8 days [days 0–2: 10% FBS DMEM with 0.5 mM 3-isobutyl-1-methyl-2,6(1H,3H)-purinedione, 10 μg/ml insulin, and 1 μM dexamethasone; days 2–4: 10% FBS DMEM with 10 μg/ml insulin; days 4–8: 10% FBS DMEM only], as described (17).

In the eicosanoid profiling experiments, culture media were collected every 2 days and cells were collected on day 0 and day 8. In the treatment experiments, cells were differentiated for 8 days and concurrently treated with MS-PPOH (1, 5, 10, and 20 μM), NUDSA (1, 5, and 10 μM), 14,15-EE-8-ZE (0.1, 0.5, and 1.0 μM), or vehicle control. Cells and media were harvested and stored at −80°C for RNA/protein isolation and eicosanoid extraction.

Oil Red O staining

On day 8, 3T3-L1 cells were washed in PBS, fixed in 4% (w/v) formaldehyde for 30 min, and then washed twice in PBS. The cells were stained with 0.2% Oil Red O in 60% 2-propanol for 15 min and washed twice with PBS, as described (17). Images were obtained with a bright field microscope equipped with an image recorder under a 20× lens. In order to quantify lipid accumulation, the Oil Red O was eluted with 100% isopropanol for 5 min, and then quantified by spectrophotometry at an absorbance of 490 nm (BioTek Instruments).

Animals

All experiments were performed in adult male mice on a C57BL/6 background. WT C57BL/6 mice were purchased from Jackson Laboratory (Bar Harbor, ME). A colony of mice with targeted disruption of *Ephx2* (*Ephx2*$^{-/-}$) was rederived and backcrossed onto a C57BL/6 genetic background for more than 10 generations and genotyped by PCR, as described previously (18, 19). All mice had free access to food and water, and were housed in controlled conditions for temperature and humidity using a 12 h light-dark cycle. All experiments were completed in accordance with the US National Institutes of Health (NIH) Guide for the Care and Use of Laboratory Animals, and were approved by the Institutional Animal Care and Use Committee.

Induction of obesity in mice

In experiment A, WT C57BL/6 mice (age 8–10 weeks) received a low-fat control diet [D12450B (10% kcal fat)], a high-fat "Western" diet [D12079B (41% kcal fat)], or a "very" HFD [VHFD, D12492 (60% kcal fat)] for 4 weeks (n = 6/group). Each diet is commercially available (Research Diets, New Brunswick, NJ), and is not enriched with arachidonic acid (<1 g per kg in each diet). In experiment B, WT mice (age 8–10 weeks) were fed the VHFD for 4 weeks, and received EET-A continuously in the drinking water (100 mg/l), or vehicle control (water), over the course of the experiment (n = 4–8/group). In experiment C, WT mice (age 8–10 weeks) were fed the VHFD for 2 weeks, and received either NUDSA (15 mg·kg^{-1}·day^{-1}) or vehicle (10% ethanol) once daily via intraperitoneal injection over the course of the experiment (n = 6/group). In experiment D, *Ephx2*$^{-/-}$ and corresponding WT control mice (age 16–20 weeks) were fed the "Western" diet (n = 11–14/group) for either 4 or 8 weeks.

In each experiment, body weight and food consumption were monitored weekly. Mice were euthanized by CO_2 inhalation, and epididymal white adipose tissue (eWAT) was harvested and weighed; one part of the tissue was snap-frozen in liquid nitrogen and stored at −80°C, while the remainder was fixed in 4% paraformaldehyde and embedded in paraffin for histological analysis.

Eicosanoid extraction and measurements

Eicosanoid metabolites were extracted from 3T3-L1 culture medium and mice eWAT by solid-phase extraction and quantified by HPLC-MS/MS, as described (20). Briefly, culture medium (3 ml) was spiked with internal standard [3 ng PGE_2-d_4, 10,11-DiHN, and 10(11)-EpHep (Cayman)], and then acidified with 330 μl of 1% acetic acid in 50% methanol. Frozen eWAT (50 mg) was homogenized in 400 μl ice-cold methanol with 0.1% acetic acid and internal standard for 10 min, centrifuged at 10,000 rpm for 10 min at 4°C, and the pellets were re-extracted with 100 μl of ice-cold methanol with 0.1% of acetic acid. The supernatants were combined with 2 ml of water and shaken. Following serial passage through HyperSep Retain SPE columns (Thermo Scientific, Bellefonte, PA), the columns were washed and then eluted with 0.5 ml of methanol and 1 ml of ethyl acetate

into glass tubes with 10 μl of trapping solution (30% glycerol in methanol). The eluates were dried under N_2 and reconstituted in 50 μl of 30% ethanol.

Online LC of extracted samples was performed with an Agilent 1200 series capillary HPLC (Agilent Technologies, Santa Clara, CA). Separations were achieved using a Halo C18 column (2.7 μm, 100 × 2.1 mm; MAC-MOD Analytical, Chadds Ford, PA), which was held at 50°C and a flow rate of 400 μl/min. Mobile phase A was 0.1% acetic acid in 85:15 water:acetonitrile. Mobile phase B was 0.1% acetic acid in acetonitrile. Gradient elution was used and the mobile phase was varied as follows: 20% B at 0 min, ramp from 0 to 5 min to 40% B, ramp from 5 to 7 min to 55% B, ramp from 7 to 13 min to 64% B. From 13 to 19 min the column was flushed with 100% B at a flow rate of 550 μl/min before being returned to starting conditions and equilibrated for 6 min. Samples were solvated in 50 μl of 30% ethanol and injected in triplicate at 10 μl per injection.

Electrospray ionization MS/MS was used for detection. Analyses were performed on an MDS Sciex API 3000 equipped with a TurboIonSpray source (Applied Biosystems, Foster City, CA). Turbo desolvation gas was heated to 425°C at a flow rate of 6 l/min. All analytes were monitored simultaneously in a scheduled multiple reaction monitoring experiment as negative ions at parent ion-product ion mass/charge ratio pairs and retention times. The relative response ratios of each analyte were used to calculate concentrations, while correcting for surrogate losses via quantification relative to internal standards. Cell medium concentrations were normalized to cell density. Adipose tissue concentrations were normalized to tissue weight. The sum concentration of EETs (14,15-EET, 11,12-EET, and 8,9-EET), dihydroxyeicosatrienoic acids (DHETs) (14,15-DHET, 11,12-DHET, 8,9-DHET, and 5,6-DHET), and total EETs+DHETs were calculated as biomarkers CYP epoxygenase metabolic function (19, 21).

RNA isolation and quantitative RT-PCR

Total 3T3-L1 cellular eWAT and brown adipose tissue (BAT) RNA were isolated using the RNeasy Miniprep kit (Qiagen, Valencia, CA). Total RNA (2 μg) was reverse transcribed to cDNA, as described (19). Expression of murine *Cyp2j5* (Mm00487292_m1), *Cyp2j9* (Mm00466423_m1), *Cyp2c29* (Mm00725580_s1), *Cyp2c44* (Mm01197184_m1), *Cyp2c55* (Mm00472168_m1), *Ephx2* (Mm01313813_m1), *Ephx3* (Mm01345663_m1), *PPARγ* (Mm01184322_m1), *C/EBPα* (Mm00514283_s1), *SREBP1c* (Mm00550338_m1), *LPL* (Mm00434764_m1), fatty acid binding protein 4 (*Fabp4*) (Mm00445878_m1), *ACC1* (Mm01304257_m1), *FAS* (Mm00662319_m1), *Tnfa* (Mm00443258_m1), uncoupling protein 1 (*UCP1*) (Mm01244861_m1), *Actb* (Mm00607939_s1), and *GAPDH* (Mm99999915_g1) were quantified using TaqMan® Assays on Demand (Applied Biosystems). The efficiency of each quantitative RT-PCR (qRT-PCR) probe for the eicosanoid metabolism genes was previously calculated over a range of cDNA amounts (1–100 ng), and was equivalent for all probes (22). Gene expression was normalized to GAPDH or β-actin and expressed relative to control using the $2^{-\Delta\Delta Ct}$ method (23).

Immunoblotting

Total 3T3-L1 cell lysates were prepared and the protein concentration was quantified, as described (24). Total protein (30 μg) was resolved and separated by 10% NuPAGE Bis-Tris gels, and then transferred to nitrocellulose membranes (Invitrogen). Membranes were blocked in 5% nonfat milk in TBS for 2 h at room temperature, incubated with anti-Cyp2j9 (1:1,000), anti-Cyp2c55 (1:1,000), anti-sEH (1:1,000), or anti-GAPDH (1:4,000) at 4°C overnight, washed, and then incubated with the appropriate horseradish peroxidase-conjugated secondary antibody (Santa Cruz Biotechnology). Immunoreactive bands were detected by chemiluminescence using the ECL Western blotting substrate (Thermo Scientific). The density of the immunoreactive bands was analyzed using ImageJ software (NIH).

CYP epoxygenase and sEH activity assay

In order to quantify CYP epoxygenase metabolic activity, 3T3-L1 preadipocytes and mature adipocytes were seeded in 12-well plates, supplemented with 1 ml of medium containing 10 μM arachidonic acid for 30 min (n = 4/group), and then EET and DHET concentrations in the medium were quantified by HPLC-MS/MS. Sum EET+DHET and sum EET concentrations were calculated and normalized to cell density. In order to quantify cellular sEH metabolic activity, 25 ng 14,15-EET was incubated with 1 μg total cell lysate from 3T3-L1 preadipocytes or mature adipocytes in a 0.1 ml volume of PBS plus 0.1 mg/ml BSA for 10 min at 37°C, as described (25). The reactions were stopped with 1 ml of ice-cold ethyl acetate, spiked with internal standard, and then evaporated to dryness under nitrogen gas. The residue was reconstituted in 30% ethanol, and EET and DHET concentrations were quantified by HPLC-MS/MS. The 14,15-EET:14,15-DHET ratio was calculated as a biomarker of sEH metabolic activity (26).

eWAT histology

Paraffin-embedded eWAT tissue underwent serial interrupted sectioning (5 μm sections, 100 μm apart), and then were stained with hematoxylin and eosin (H&E) and scanned into digital images (ScanScope CS; Aperio, Vista, CA). The average adipocyte size per 10× field was quantified using ImageJ software (NIH) and the MRI adipocyte tool, as described (27). An average value across nine nonoverlapping fields (three fields/section × three sections/mouse) was calculated for each mouse.

Body composition and metabolic measurements

Body composition was measured in live mice without anesthesia by quantitative magnetic resonance using an EchoMRI-100 whole body composition analyzer (EchoMRI, Houston, TX), as described (28). Fat and lean mass were quantified at baseline, week 2 and week 4, and expressed as a percentage of total body weight. At week 3, oxygen consumption (VO_2) and carbon dioxide production (VCO_2) were quantified by indirect calorimetry in unrestrained individually housed mice using a TSE LabMaster system (TSE Systems, Chesterfield, MO), which also quantifies food and water consumption (28). Measurements were obtained in 27 min intervals over 24 h, normalized to total body weight, and averaged. The respiratory exchange ratio (RER = VCO_2/VO_2) and metabolic rate [= (3.815 + 1.232 × RER) × VO_2] were calculated.

Glucose tolerance test

Mice were fasted 6 h, and then dosed with 20% D-glucose by intraperitoneal injection (week 4: 2 mg/g body weight; week 8: 1 mg/g body weight). Whole blood glucose concentrations were measured before and 20, 30, 60, 90, and 120 min following dosing using the Accu-Chek Aviva Plus glucometer (Roche Diagnostics GmbH, Mannheim, Germany), as described (29). Due to progressive glucose intolerance and the upper limit of detection of the glucometer (600 mg/dl), a lower glucose dose was used at 8 weeks. The area under the glucose concentration-time curve (glucose $AUC_{0–120min}$) was calculated using the trapezoidal method.

Metabolomic analysis

A total of 33 distinct eicosanoid metabolites were quantifiable by HPLC-MS/MS in the 3T3-L1 cell culture media. A principal components analysis (PCA) was employed in the MetaboAnalyst 2.0 web portal (30) to identify whether changes in the global eicosanoid profile occurred during adipocyte differentiation (n = 4/time-point). The PCA results were displayed as score plots to visualize sample clustering and to indicate sample differences across the differentiation time-course. The relative impact of adipocyte differentiation on eight self-defined eicosanoid metabolic pathways (**Table 1**) was evaluated by quantitative enrichment analysis, which is based on the global test algorithm and uses a generalized linear model to estimate a Q-statistic for each metabolite set. Pathways were considered significantly enriched when $P < 0.00625$ (= 0.05/8), and the corresponding false discovery rate (FDR) was <5%.

Statistical analysis

All data were expressed as mean ± SEM. A one-way ANOVA was employed to analyze the differences across treatment groups followed by a post hoc Dunnett's test to evaluate whether treatment differences existed relative to the control group. A post hoc Wilcoxon rank-sum test was used for data that were not normally distributed. Differences in the glucose concentration-time profile were determined using general linear model repeated-measures ANOVA, and a post hoc Scheffe's test. Correlations were evaluated using the Spearman rank correlation where indicated. Statistical analysis was performed using SAS-JMP 6.0 or SAS 9.2 software (SAS Institute, Cary, NC), and $P < 0.05$ was considered significant.

RESULTS

Adipocyte differentiation suppresses CYP epoxygenase-derived EETs in vitro

We first investigated the effect of adipocyte differentiation over time on the global eicosanoid profile in 3T3-L1 adipocytes. Oil Red O staining (**Fig. 1A**) and *Fabp4* mRNA levels (Fig. 1B) confirmed the differentiation of preadipocytes into mature adipocytes. The PCA analysis demonstrated a clear separation of the global eicosanoid profile across preadipocytes and differentiated adipocytes (Fig. 1C). Notably, the CYP epoxygenase-derived arachidonic acid pathway was the most significantly changed metabolite set during adipocyte differentiation (Table 1). The sum EET, sum DHET, and sum EET+DHET concentrations were significantly reduced in 3T3-L1 mature adipocytes compared with preadipocytes (Fig. 1D). This was apparent after 2 days and sustained throughout the entire differentiation period (Fig. 1E–G).

We subsequently assessed expression of key CYP epoxygenases (*Cyp2j5*, *Cyp2j9*, *Cyp2c29*, *Cyp2c44*, and *Cyp2c55*) and epoxide hydrolases (*Ephx2* and *Ephx3*) (**Fig. 2A**). Cyp2j9 and Cyp2c55 protein levels were reduced and sEH protein was increased in mature adipocytes compared with preadipocytes (Fig. 2B–D). Consistent with the expression data, the capacity to generate EETs and DHETs (CYP epoxygenase metabolic activity) was significantly lower (Fig. 2E, F) and the capacity to hydrolyze 14,15-EET to 14,15-DHET (sEH metabolic activity) was significantly higher (Fig. 2G) in mature adipocytes. These findings indicate that induction of adipogenesis dysregulates the CYP epoxygenase pathway and suppresses the bioavailability of EETs in adipocytes.

Diet-induced obesity suppresses CYP epoxygenase-derived EETs in adipose tissue in vivo

Mice fed two distinct HFDs each exhibited a significant increase in total body weight gain (**Fig. 3A**) and eWAT weight (Fig. 3B) at 4 weeks. High-fat feeding significantly reduced EET and DHET levels in eWAT, in both models, compared with controls (Fig. 3C, D). Furthermore, eWAT EET levels inversely correlated with body weight gain ($r = -0.633$, $P = 0.005$), adipose tissue weight (Fig. 3E), key biomarkers of adipogenesis [SREBP1c ($r = -0.733$, $P = 0.001$), C/EBPα ($r = -0.506$, $P = 0.032$), and PPARγ ($r = -0.485$, $P = 0.041$) mRNA levels in eWAT], and activation of the inflammatory response in eWAT (Fig. 3F). Taken together, these results are consistent with our in vitro experiments and indicate that induction of adipose tissue expansion suppresses EET levels in eWAT.

TABLE 1. Metabolite set enrichment analysis in 3T3-L1 preadipocytes and differentiated adipocytes

Pathways (8)	Metabolites (33)	Total	Q Statistic	Raw *P* Value	Holm *P* Value[a]	FDR[a]
CYP epoxygenase-derived arachidonic acid metabolites	8,9-EET, 11,12-EET, 14,15-EET, 5,6-DHET, 8,9-DHET, 11,12-DHET, 14,15-DHET	7	86.60	1.69E-16	1.35E-15	1.35E-15
CYP epoxygenase-derived linoleic acid metabolites	9,10-EpOME, 12,13-EpOME, 9,10-DiHOME, 12,13-DiHOME	4	85.07	3.61E-15	2.53E-14	1.47E-14
Lipoxygenase-derived arachidonic acid metabolites	15-HETE, 12-HETE, 11-HETE, 8-HETE, 5-HETE	5	84.86	7.39E-14	4.43E-13	1.97E-13
Lipoxygenase-derived linoleic acid metabolites	9,12,13-TriHOME, 9,10,13-TriHOME, 13-HODE, 9-HODE	4	37.21	1.50E-05	7.49E-05	2.99E-05
CYP hydroxylase-derived arachidonic acid metabolites	19-HETE, 20-HETE	2	41.72	5.82E-05	2.33E-04	9.31E-05
Cyclooxygenase-derived arachidonic acid metabolites	6-keto-PGF1$_\alpha$, TxB2, PGF2$_\alpha$, PGD2, PGE2, 8-iso-PGF2$_\alpha$, PGB2	7	21.53	5.46E-04	1.64E-03	7.28E-04
CYP epoxygenase-derived docosahexaenoic acid metabolites	19,20-DiHDPA, 19,20-EpDPE	2	14.93	0.029	0.058	0.033
CYP epoxygenase-derived eicosapentaenoic acid metabolites	17,18-DiHETE, 17,18-EpETE	2	1.94	0.447	0.447	0.447

DiHDPA, dihydroxydocosapentaenoic acid; DiHETE, dihydroxyeicosatetraenoic acid; DiHOME, dihydroxyoctadecenoic acid; EpDPE, epoxydocosapentaenoic acid; EpETE, epoxyeicosatetraenoic acid; EpOME, epoxyoctadecenoic acid; PG, prostaglandin; TriHOME, trihydroxyoctadecenoic acid; Tx, thromboxane.

[a]The pathways (rank-ordered) were considered significantly enriched when the Holm $P < 6.25E-03$ and FDR <5%.

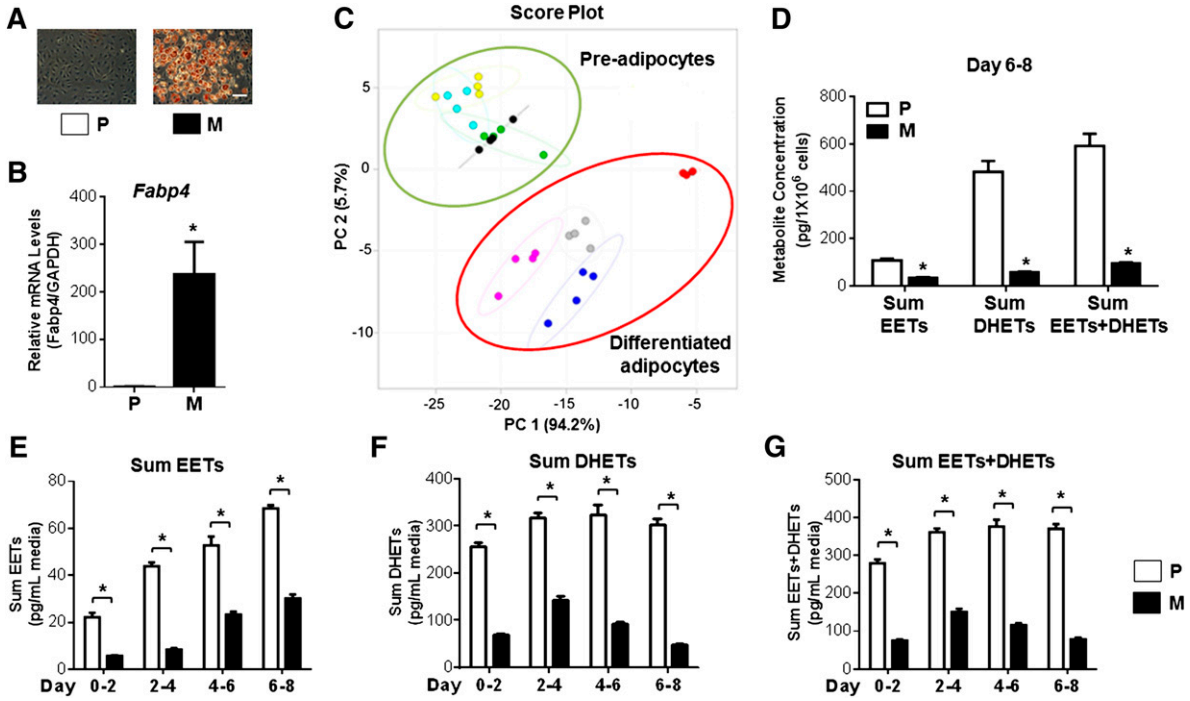

Fig. 1. EET levels are reduced in 3T3-L1 mature adipocytes compared with preadipocytes. A: 3T3-L1 preadipocytes (P) and mature adipocytes (M) (differentiated for 8 days) were fixed and stained by Oil Red O (scale bar = 40 μm). B: *Fabp4* mRNA levels were quantified by qRT-PCR (n = 3 per group) to confirm adipocyte differentiation. C: The culture medium was collected every 2 days during the differentiation period, and a total of 33 distinct eicosanoid metabolites were quantified by HPLC-MS/MS. A PCA demonstrates a clear separation of the global eicosanoid profiles across preadipocytes and differentiated adipocytes. Preadipocytes are shown as green dots (days 0–2), cyan dots (days 2–4), yellow dots (days 4–6), and black dots (days 6–8); differentiated adipocytes are shown as red dots (days 0–2), blue dots (days 2–4), gray dots (days 4–6), and purple dots (days 6–8). D: Specific evaluation of the CYP epoxygenase-derived arachidonic acid metabolite pathway demonstrated that the sum EET, sum DHET, and sum EET+DHET concentrations normalized by cell density (days 6–8) were significantly reduced in 3T3-L1 mature adipocytes compared with preadipocytes (n = 4 per group). E–G: The reduction of the sum EET (E), sum DHET (F), and sum EET+DHET (G) concentrations were apparent after 2 days and sustained throughout the entire differentiation period (n = 4 per group). $*P < 0.05$ versus preadipocytes.

Modulation of the CYP epoxygenase pathway alters adipocyte differentiation in vitro

In order to elucidate the functional role of the CYP epoxygenase pathway in the regulation of adipogenesis, we first differentiated 3T3-L1 preadipocytes to mature adipocytes in the presence of the CYP epoxygenase inhibitor, MS-PPOH. Administration of MS-PPOH dose-dependently increased lipid accumulation in mature adipoctyes (**Fig. 4A, B**). Due to the instability of exogenously administered EETs, follow-up experiments were completed using the stable EET analogs, NUDSA and 14,15-EE-8(Z)-E. Administration of NUDSA (Fig. 4C, D) and 14,15-EE-8(Z)-E (Fig. 4E, F) each attenuated the differentiation of 3T3-L1 preadipocytes into mature adipocytes. Furthermore, 14,15-EE-8(Z)-E dose-dependently downregulated the induction of the adipocyte differentiation associated transcription factors PPARγ, C/EBPα, and SREBP1c (**Fig. 5A–C**), and the adipocyte differentiation-associated genes LPL, ACC1, FAS, and Fabp4 (Fig. 5D–G). Altogether, these findings implicate the CYP epoxygenase pathway as a key functional regulator of adipogenesis.

Administration of an EET analog suppresses adipocyte differentiation in the early phase

Due to the marked reduction of EET levels during the early phases of adipocyte differentiation, we sought to determine whether the early phase adipocyte differentiation was most sensitive to the anti-adipogenic effects of EET analog administration. Treatment with 14,15-EE-8(Z)-E during the first 2 (days 0–2) or 4 (days 0–4) days markedly attenuated adipocyte differentiation to a similar extent as treatment throughout the entire differentiation period (days 0–8) (**Fig. 6A, B**). However, initiation of treatment of on day 2, day 4, or day 6 elicited dramatically less to no effect on adipocyte differentiation. Furthermore, treatment with 14,15-EE-8(Z)-E during days 0–2, 0–4, and 0–8 dramatically decreased the induction of PPARγ, C/EBPα, and SREBP1c mRNA levels at day 2 (the early phase), day 4 (the intermediate phase), and day 8 (the late phase) compared with vehicle control-treated cells (Fig. 6D). Consistent with the lipid accumulation data, however, initiation of treatment with 14,15-EE-8(Z)-E beyond the early phase (on day 2, day 4, or day 6) had dramatically less to no effect (Fig. 6C). These findings demonstrate that EET analogs significantly attenuate adipocyte maturation via inhibition of the early phase of adipogenesis.

Promoting the effects of EETs elicits protective effects in diet-induced obesity in vivo

Administration of EET-A, an EET analog conducive to administration in the drinking water (14), significantly attenuated HFD-evoked body weight gain (**Fig. 7A**) and

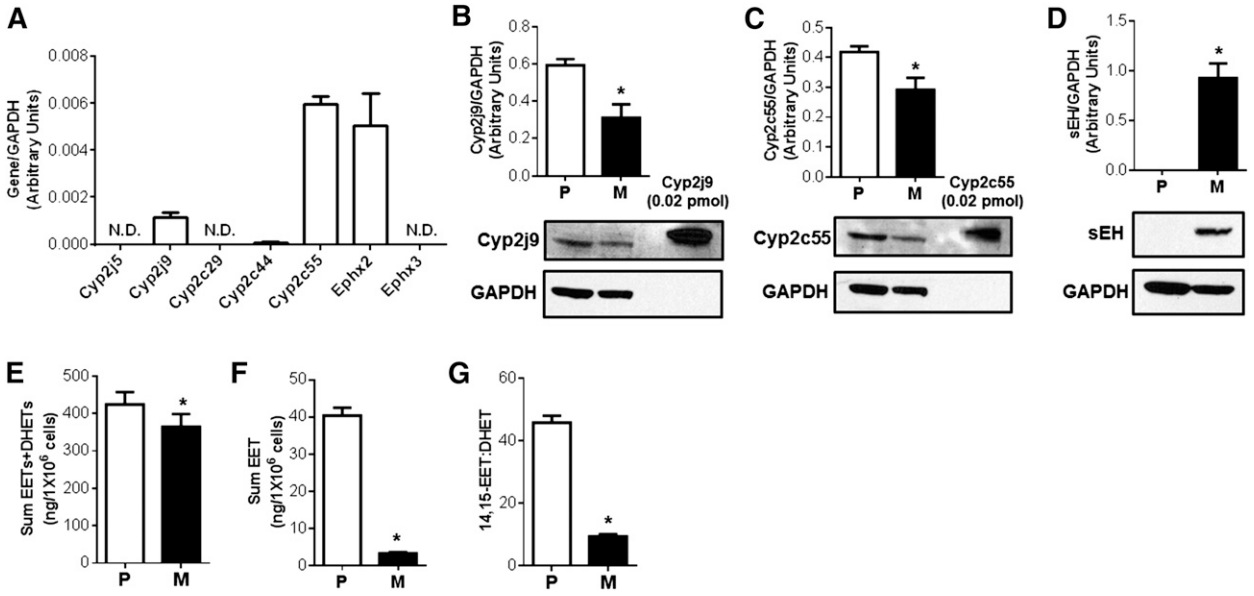

Fig. 2. Characterization of CYP epoxygenase and sEH expression and activity in 3T3-L1 preadipocytes and mature adipocytes. 3T3-L1 preadipocytes (P) and mature adipocytes (M) (differentiated for 8 days) were harvested. A: The relative abundance of CYP epoxygenase and epoxide hydrolase mRNA levels were quantified in 3T3-L1 preadipocytes (N.D., not detected) and normalized to GAPDH (n = 3 per group). B–D: Representative immunoblot and densitometry analysis demonstrate lower Cyp2j9 (B) and Cyp2c55 (C) and higher sEH (D) protein expression in mature adipocytes compared with preadipocytes (n = 3 per group). Sum EET+DHET (E) and sum EET (F) concentrations following incubation with 10 μM arachidonic acid for 30 min (biomarker of CYP epoxygenase metabolic activity). G: The 14,15-EET:DHET ratio following incubation with 25 ng 14,15-EET for 10 min [biomarker of sEH activity (lower ratio indicative of higher activity)] were each significantly reduced in mature adipocytes (n = 4 per group). *$P < 0.05$ versus preadipocytes.

adipose tissue expansion (Fig. 7B–D) compared with vehicle-treated controls. These effects were not accompanied with a reduction in food consumption (Fig. 7E). Assessment of metabolic capacity illustrated that EET-A administration attenuated the HFD-evoked suppression of energy expenditure compared with vehicle-treated controls (Fig. 7F–I), although the observed increase in O_2 consumption (Fig. 7F, $P = 0.149$) and metabolic rate (Fig. 7I, $P = 0.089$) was not statistically significant. EET-A treatment also significantly increased expression of UCP1 in BAT (Fig. 7J).

Furthermore, EET-A treatment significantly attenuated the induction of systemic glucose intolerance (Fig. 7K, L). Although EET-A did not significantly reduce fasting (Fig. 7K; time 0) or fed (Fig. 7M) blood glucose concentrations, high-fat feeding did not significantly increase fasting ($P = 0.107$) or fed ($P = 0.350$) glucose levels compared with the control diet, illustrating the prediabetic state (i.e., obesity and glucose intolerance without overt diabetes) at 4 weeks.

Administration of NUDSA, an EET analog conducive to repeated dosing in vivo (13), also significantly attenuated HFD-evoked weight gain (**Fig. 8A**) compared with vehicle-treated controls without affecting average food consumption (16.1 ± 0.8 g/week/mouse vs. 17.5 ± 1.2 g/week/mouse, respectively, $P = 0.468$). Furthermore, and consistent with the effects elicited by EET-A, the induction of eWAT mass (Fig. 8B), adipocyte hypertrophy (Fig. 8C, D), and expression of the adipogenic markers PPARγ and LPL in eWAT (Fig. 8E) were significantly attenuated and expression of UCP1 in BAT was significantly augmented (Fig. 8F) by NUDSA treatment. In a parallel series of experiments, mice with targeted disruption of *Ephx2* and significantly higher endogenous EETs in eWAT (14,15-EET:DHET: 4.27 ± 0.54 vs. 0.13 ± 0.06, respectively, $P < 0.05$ vs. WT) underwent HFD feeding for 4–8 weeks. Although a significant decrease in body weight gain was not observed (**Fig. 9A, C**), *Ephx2*$^{-/-}$ mice exhibited a significantly attenuated induction of PPARγ and LPL mRNA levels in eWAT (Fig. 9B, D) and systemic glucose intolerance (Fig. 9E–H) compared with WT controls at both 4 and 8 weeks. Taken together, these results indicate that therapeutic restoration of EETs elicits metabolic protective effects in diet-induced obesity in vivo.

DISCUSSION

Adipogenesis plays a key role in the initiation and progression of obesity and obesity-associated metabolic diseases. Although CYP epoxygenase-derived EETs possess potent protective effects in the cardiovascular system (7, 8), the functional role of EETs in the regulation of adipogenesis and the pathogenesis of obesity remains poorly understood. In the present investigation, we demonstrated that: *a*) adipogenesis and obesity-associated adipose expansion significantly dysregulate the CYP epoxygenase pathway and evoke a marked suppression of EET levels in adipose tissue; and *b*) potentiating the effects of EETs elicits potent anti-adipogenic and anti-obesity effects both in vitro and in vivo. Collectively, these findings suggest that suppression of EET bioavailability in adipose tissue is a key pathological consequence in the early stages of obesity,

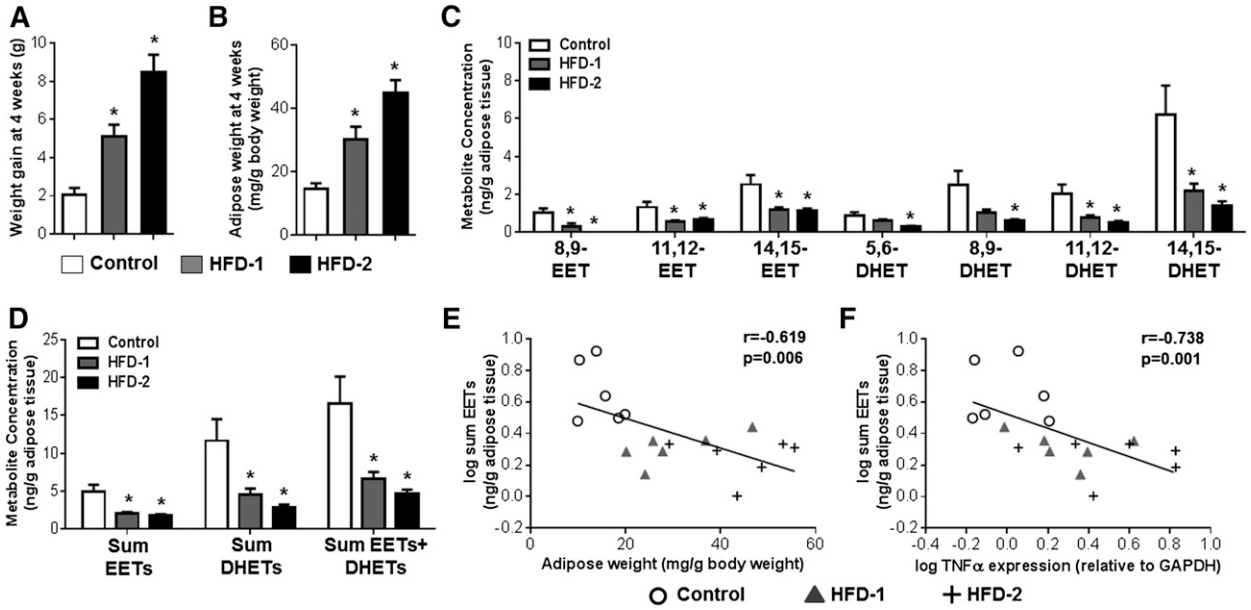

Fig. 3. Induction of obesity with HFD feeding significantly suppressed adipose EET and DHET levels in mice. Mice were fed a low-fat control diet [Control; D12450B (10% kcal fat)], a high-fat Western diet [HFD-1; D12079B (41% kcal fat)], and a VHFD [HFD-2; D12492 (60% kcal fat)] for 4 weeks (n = 6 per group) to induce obesity and adipose tissue expansion. A–D: HFD-1 and HFD-2 each increased weight gain (A) and eWAT weight (normalized to body weight) (B), and suppressed eWAT EET and DHET concentrations [individual regioisomer (C) and sum total (D); normalized to tissue weight] compared with the control diet. Except for 8,9-EET levels, which were below the detection limit in three of six Western and six of six VHFD-fed mice, all EET and DHET regioisomers were detectable in the eWAT of lean and obese animals. E–F: eWAT EET concentration exhibited a significant inverse correlation with eWAT weight (E) and TNFα mRNA levels in eWAT (quantified by qRT-PCR and normalized to GAPDH) (F). The Spearman's rank correlation coefficient and accompanying *P* value are provided. $*P < 0.05$ versus control diet group.

and strategies that promote the protective effects of EETs in adipose tissue offers enormous therapeutic potential for obesity-associated metabolic diseases.

We recently reported that obesity was associated with significantly lower circulating EET levels in humans with established cardiovascular disease (26). Although prior studies have demonstrated that experimental induction of obesity reduces EETs in liver, kidney, and mesenteric arteries (21, 31), as well as alters cyclooxygenase-mediated prostaglandin biosynthesis and lipoxygenase-mediated leukotriene biosynthesis in adipose tissue (32, 33), the impact of obesity on EET bioavailability in adipose tissue has not been rigorously investigated. Consequently, we employed a metabolomic approach to characterize the global eicosanoid profile during adipocyte differentiation in 3T3-L1 cells. Adipocyte maturation significantly altered the global eicosanoid profile; however, the CYP epoxygenase-derived EETs and DHETs were markedly suppressed and the most significantly changed metabolites compared with parallel pathways. Moreover, Cyp2j9 and Cyp2c55 expression were suppressed and sEH expression was induced in mature adipocytes, consistent with prior reports in mesenchymal stem cells and 3T3-L1-derived adipocytes (34, 35). Our studies also demonstrate a significant functional suppression of CYP epoxygenase (decreased EET+DHET formation) and induction of epoxide hydrolase (increased 14,15-EET hydrolysis) metabolic activity in mature adipocytes, suggesting that the adipogenesis-evoked suppression of EET levels is secondary to both suppressed Cyp2c/2j-mediated biosynthesis and increased sEH-mediated hydrolysis. Importantly, consistent with our experiments in cultured 3T3-L1 adipocytes and a recent report in rats (9), induction of obesity and adipose tissue expansion in mice with high fat feeding significantly suppressed EET concentrations in eWAT. Moreover, we observed a marked suppression of each EET and DHET regioisomer in eWAT, which were inversely correlated with body weight gain, eWAT weight, and adipogenesis-related transcription factor expression. We also observed a significant inverse correlation between proinflammatory cytokine expression and EET levels in eWAT. Our previous studies have demonstrated that activation of the innate immune inflammatory response suppresses hepatic EET biosynthesis (22). Given the integral contribution of inflammation in visceral adipose tissue to the pathogenesis of obesity (4), activation of obesity-associated inflammatory responses may also drive the suppression of EET bioavailability in adipose tissue. However, future studies are needed to elucidate these effects and the underlying mechanisms. It is important to note that we did not quantify EET concentrations in multiple adipose tissue depots, which is a limitation. Comprehensive evaluation of the relative impact of obesity on EET levels across distinct adipose tissue depots, as well as across species, remains an important future direction for this line of investigation.

In addition to the observed suppression of EET bioavailability during adipocyte differentiation, further inhibition of EET biosynthesis via administration of a CYP epoxygenase inhibitor significantly accelerated adipogenesis. Collectively, these data suggest that CYP-derived EETs play an

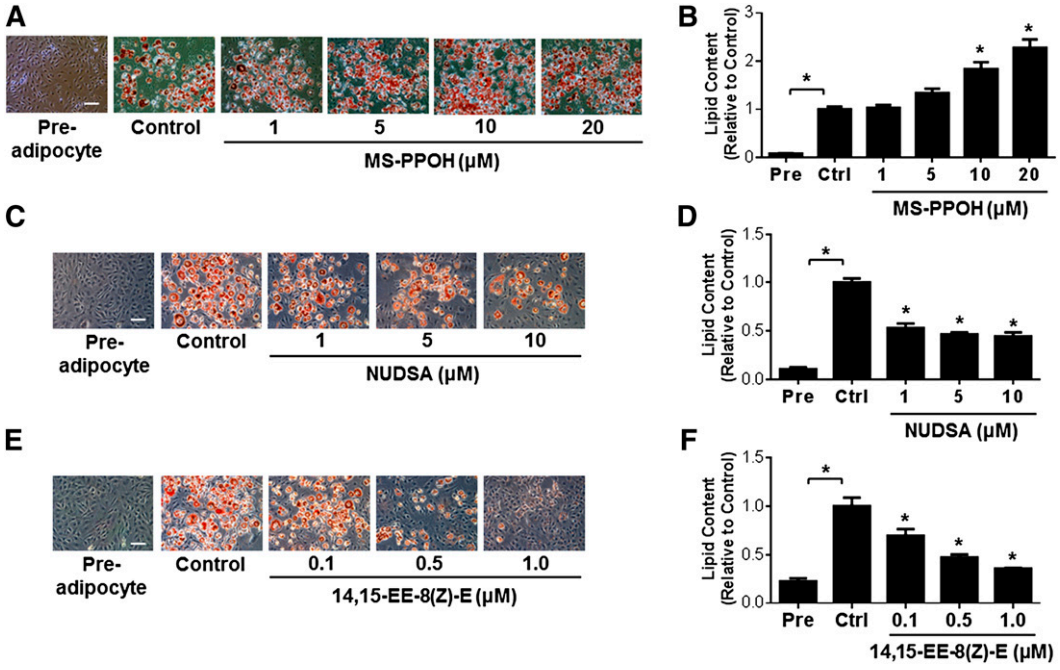

Fig. 4. Modulation of the CYP epoxygenase pathway alters adipocyte differentiation of 3T3-L1 cells. 3T3-L1 cells were induced to differentiate while concurrently being treated with MS-PPOH (1, 5, 10, and 20 μM), NUDSA (1, 5, and 10 μM), 14,15-EE-8(Z)-E (0.1, 0.5, and 1.0 μM), or vehicle for 8 days. A, C, E: Representative images of Oil Red O-stained adipocytes treated with MS-PPOH (A), NUDSA (B), and 14,15-EE-8(Z)-E (C) are provided (scale bar = 40 μm). B, D, F: Cellular lipid content was quantified by spectrophotometry after elution with isopropanol, and then normalized to the vehicle control group (n = 3–6 per group). All data are expressed relative to the vehicle control group. *$P < 0.05$ versus vehicle control. Pre, preadipocyte; Ctrl, control.

integral functional role in the regulation of adipogenesis. Furthermore, two distinct EET analogs (14,15-EE-8(Z)-E and NUDSA) each dose-dependently inhibited lipid accumulation and adipocyte differentiation-associated gene expression, clearly demonstrating that pharmacologic promotion of EETs elicits potent anti-adipogenic effects. Other EET analogs have been reported to attenuate adipogenesis in human mesenchymal stem cell-derived adipocytes (34, 36, 37). Taken together, these studies and our experiments demonstrate the potent anti-adipogenic

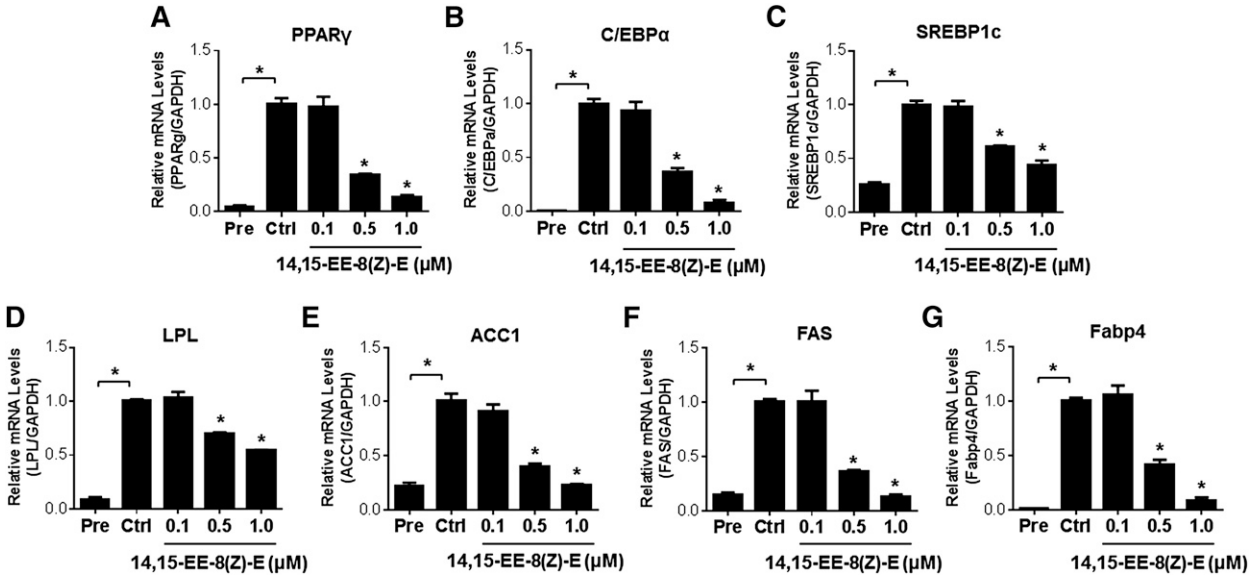

Fig. 5. Administration of the EET analog 14,15-EE-8(Z)-E reduces adipogenic gene expression in 3T3-L1 cells. 3T3-L1 cells were induced to differentiate while concurrently being treated with 14,15-EE-8(Z)-E (0.1, 0.5, and 1.0 μM) or vehicle for 8 days. PPARγ (A), C/EBPα (B), SREBP1c (C), LPL (D), ACC1 (E), FAS (F), and Fabp4 (G) mRNA levels were quantified by qRT-PCR and normalized to GAPDH (n = 3 per group). Similar results were observed after the data were normalized to β-actin (data not shown). All data are expressed relative to the vehicle control group. *$P < 0.05$ versus vehicle control. Pre, preadipocyte; Ctrl, control.

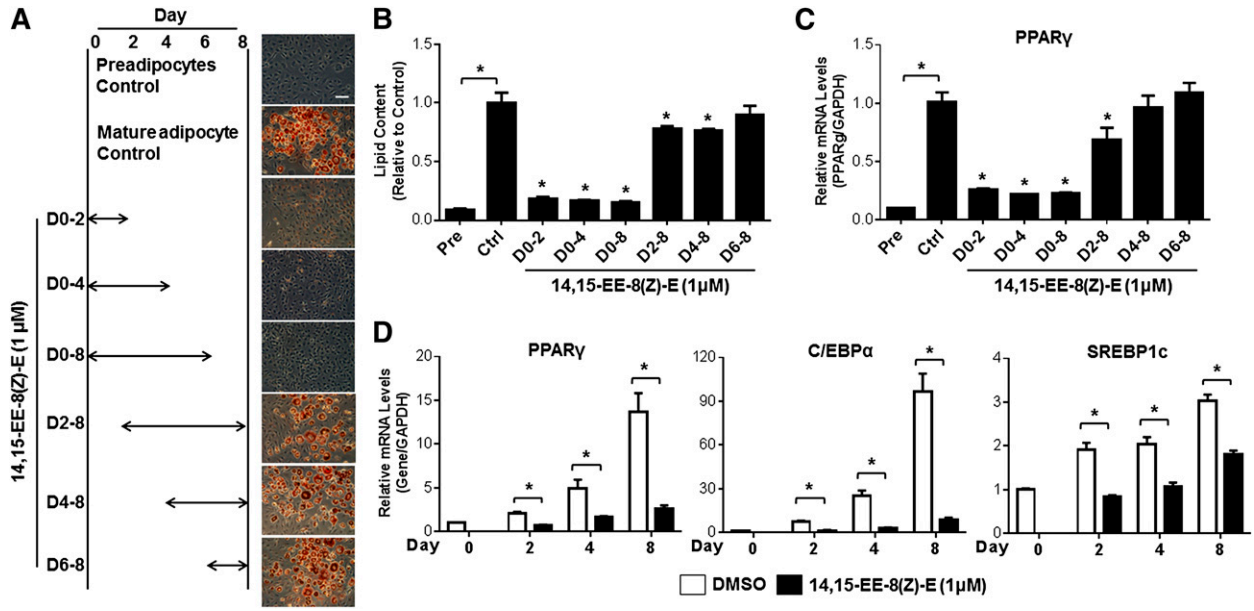

Fig. 6. The early stages of adipogenesis are critical to the anti-adipogenic effects of the EET analog, 14,15-EE-8(Z)-E. 3T3-L1 cells were differentiated to mature adipocytes for 8 days. A: 14,15-EE-8(Z)-E (1 μM) was administered during the time period indicated. Representative images of Oil Red O-stained adipocytes on day 8 are provided for each treatment group (scale bar = 40 μm). B: Cellular lipid content was quantified by spectrophotometry after elution with isopropanol, and then normalized to the vehicle control group (n = 3 per group). C: PPARγ mRNA levels were quantified by qRT-PCR in 3T3-L1 cells on day 8. 3T3-L1 cells were differentiated in the presence of 14,15-EE-8(Z)-E (1 μM) or vehicle (0.1% DMSO) control for 0–2, 0–4, or 0–8 days. D: PPARγ, C/EBPα, and SREBP1c mRNA levels were quantified by qRT-PCR on day 2, 4, or 8, respectively (n = 3 per group). The data were normalized to GAPDH and expressed relative to the vehicle control group. *$P < 0.05$ versus vehicle control. Pre, preadipocyte; Ctrl, control.

effects of multiple EET analogs in multiple cell systems. Furthermore, our experiments demonstrate for the first time that EET analog treatment elicits its anti-adipogenic effects through targeting the biochemical and cellular events in the early phase of adipogenesis, which are crucial for adipocyte differentiation (38). This was reflected by the marked and early suppression of PPARγ, C/EBPα, and SREBP1c mRNA levels that were sustained throughout the entire differentiation period. Moreover, initiation of EET analog treatment during the late phase of differentiation failed to inhibit either the induction of adipogenic transcription factor expression or lipid accumulation.

It is well-established that activation of PPARγ, C/EBPα, and SREBP1c are central mediators of adipogenesis through their regulation of lipid biosynthesis and metabolism (2, 3) Several mechanisms are known to regulate this transcriptional factor network. During the early differentiation of preadipocytes, inhibition of ERK and activation of the AMP-activated protein kinase (AMPK) and cAMP/protein kinase A (PKA) signaling pathways inhibit PPARγ, C/EBPα, and SREBP1c activation and adipocyte differentiation (39–41). Previous studies have demonstrated that promoting the effects of EETs attenuates ERK1/2 dephosphorylation in endothelial cells, activates AMPK activity in liver, and activates the cAMP/PKA pathway in the vascular system (12, 42, 43), suggesting that a complex interaction between CYP-derived EETs and multiple signaling pathways also likely exist in the early phase of adipogenesis. Future studies are needed to delineate the key signaling pathways that underlie the inhibitory effects of EETs on adipocyte differentiation.

Promoting the effects of EETs also elicited potent metabolic protective effects in vivo. Most notably, EET analog administration significantly mitigated HFD-induced weight gain, adipose tissue expansion, and adipocyte differentiation-associated gene expression. Although the attenuation of weight gain by EET analog treatment was not accompanied by a reduction in food consumption, food absorption was not quantified. Because changes in intestinal absorption of calories could contribute, at least in part, to the observed weight gain phenotypes, this is a limitation. However, EET analog administration attenuated the HFD-evoked suppression of whole-body energy expenditure and augmented expression of the mitochondrial protein carrier UCP1. UCP1, which is highly expressed in BAT and dissipates chemical energy in the mitochondria in the form of heat via fatty acid oxidation, is a critical regulator of energy expenditure in adipose tissue and dysregulation of this process is a key driver of the pathogenesis of obesity (44, 45). Taken together, these data suggest that promoting the effects of EETs attenuates adipose expansion and weight gain by enhancing metabolic efficiency in adipose tissue. The anti-obesity effects in HFD-fed mice and the anti-adipogenic effects in differentiated 3T3-L1 cells are challenging to reconcile because adipocyte hypertrophy, and not hyperplasia, has been traditionally recognized as the primary driver of adipose tissue expansion in obesity (5). It is important to note, however, recent studies have demonstrated that de novo adipogenesis also is an important contributor to HFD-induced obesity (46), highlighting the important but complex contribution of

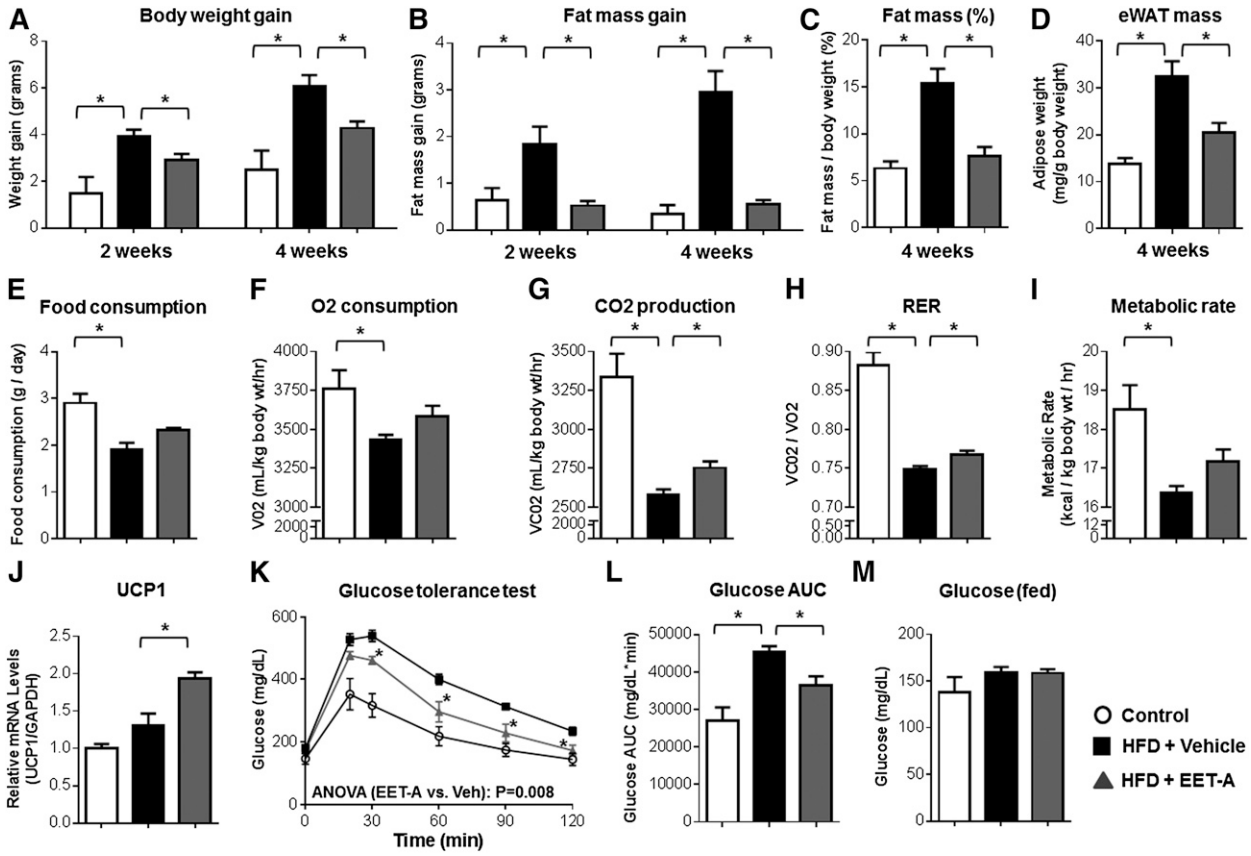

Fig. 7. The EET analog, EET-A, elicits anti-obesity effects and attenuates glucose intolerance in mice fed a HFD. Mice were fed a HFD (D12492) or control diet for 4 weeks (n = 4–8 per group). HFD-fed mice were treated with EET-A (100 mg/l in the drinking water) or vehicle control for 4 weeks. A–D: Compared with vehicle, EET-A treatment attenuated the HFD-induced increase in total body weight gain from baseline (A), fat mass gain (EchoMRI) from baseline (B), fat mass (EchoMRI) expressed as a percentage of total body weight (C), and eWAT mass at necropsy normalized by body weight (D). E: Cumulative food consumption over 24 h. F–I: Energy expenditure phenotypes, including VO_2 (F), VCO_2 (G), the RER (H), and the metabolic rate (I), were assessed at week 3. Energy expenditure phenotypes were averaged over 24 h and normalized to body weight. J: BAT mRNA levels of UCP1 were quantified by qRT-PCR, normalized to GAPDH, and expressed relative to the control diet group. K: At 4 weeks, blood glucose concentrations were quantified at baseline (fasting) and over 120 min following an intraperitoneal glucose tolerance test. The repeated measures ANOVA *P* value is provided. L: The corresponding AUC at 4 weeks was calculated. M: Blood glucose concentrations (fed) were quantified at necropsy. $^*P < 0.05$ versus HFD-vehicle.

adipogenesis to obesity. Consequently, future studies are needed to delineate the relative contribution of adipocyte hyperplasia and hypertrophy, and the underlying molecular mechanisms to the anti-obesity effects of EET analogs in vivo.

The development of glucose intolerance is a critical pathological consequence of obesity, which drives the development of type 2 diabetes (4). Administration of the EET analog, EET-A, significantly abrogated the HFD-evoked induction of glucose intolerance in vivo. Similarly, mice with targeted disruption of *Ephx2* and restored endogenous EET levels exhibited an attenuated induction of glucose intolerance following 4 and 8 weeks of high-fat feeding. In contrast to EET analog treatment, weight gain was not attenuated in $Ephx2^{-/-}$ mice. These data are consistent with a prior report illustrating improved glucose tolerance in $Ephx2^{-/-}$ mice without changes in weight gain, compared with WT controls, after 20 weeks of HFD feeding (11). The mechanisms underlying these differences, including the potential for compensatory changes secondary to gene disruption, remain unclear and warrant further investigation. Induction of adipocyte differentiation-associated transcription factor and lipogenic gene expression following high fat feeding, however, was significantly attenuated in $Ephx2^{-/-}$ mice. Multiple studies have demonstrated that inhibition of adipogenic transcriptional factor activation ameliorates HFD-induced glucose intolerance (47, 48). Moreover, early-onset glucose intolerance during high-fat feeding is primarily driven by lipid overload (49), as opposed to other mechanisms including hepatic inflammation, pancreatic dysfunction, and systemic insulin resistance, that are more pronounced in the later stages of obesity. Thus, our experiments suggest that promoting the effects of EETs in adipose tissue contribute to improved glucose tolerance during the early stages of obesity, at least in part, through attenuating the activation of pro-adipogenic gene expression; however, future studies remain necessary to

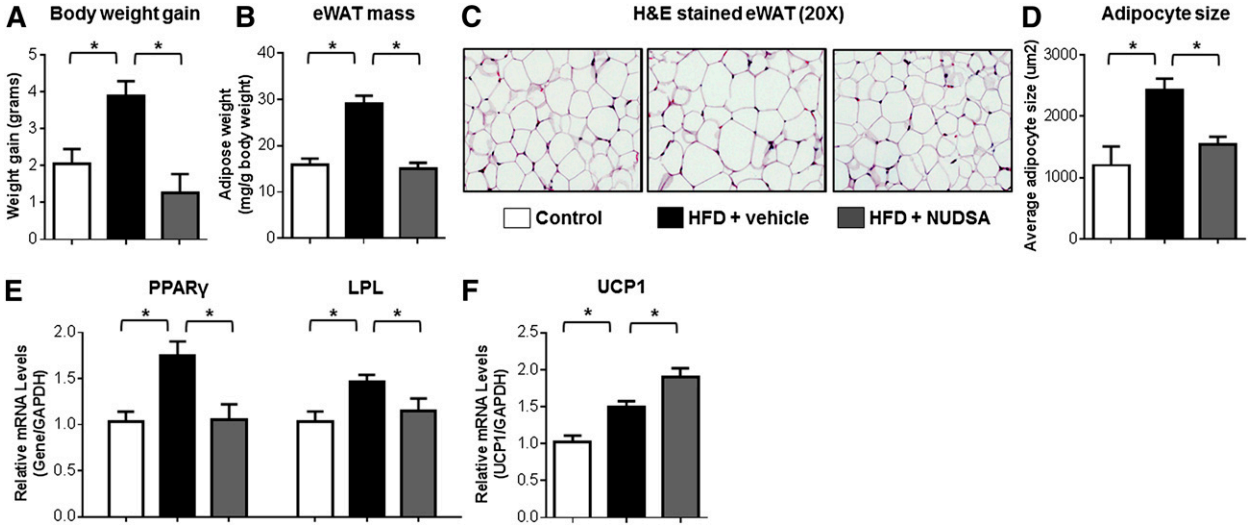

Fig. 8. The EET analog NUDSA elicits anti-obesity effects in mice fed a HFD. Mice were fed a HFD (D12492) or control diet for 2 weeks (n = 6 per group). HFD-fed mice were treated with either NUDSA (15 mg·kg^{-1}·day^{-1}) or vehicle control via intraperitoneal injection once daily for 2 weeks. A, B: Compared with vehicle, NUDSA treatment attenuated the HFD-induced increase in total body weight gain from baseline (A) and eWAT mass at necropsy normalized by body weight (B). C: Representative images of H&E-stained eWAT sections (magnification 20×) are provided. D: Average adipocyte size per 10× field was quantified using ImageJ. eWAT mRNA levels of PPARγ and LPL (E) and BAT mRNA levels of UCP1 (F) were quantified by qRT-PCR, normalized to GAPDH, and expressed relative to the control diet group. *$P < 0.05$ versus HFD-vehicle.

delineate these effects and elucidate the underlying mechanisms, and to evaluate the metabolic protective effects of EET analog treatment during the later stages of obesity.

In summary, our studies demonstrate that CYP epoxygenase-derived EETs play an integral functional role in the regulation of adipogenesis and the pathogenesis of obesity, and suggest that suppression of EET bioavailability in adipose tissue is a key pathological consequence of obesity. Therapeutic strategies that promote the protective effects of EETs in adipose tissue offer enormous potential to mitigate obesity-associated metabolic disease and its downstream pathological consequences.

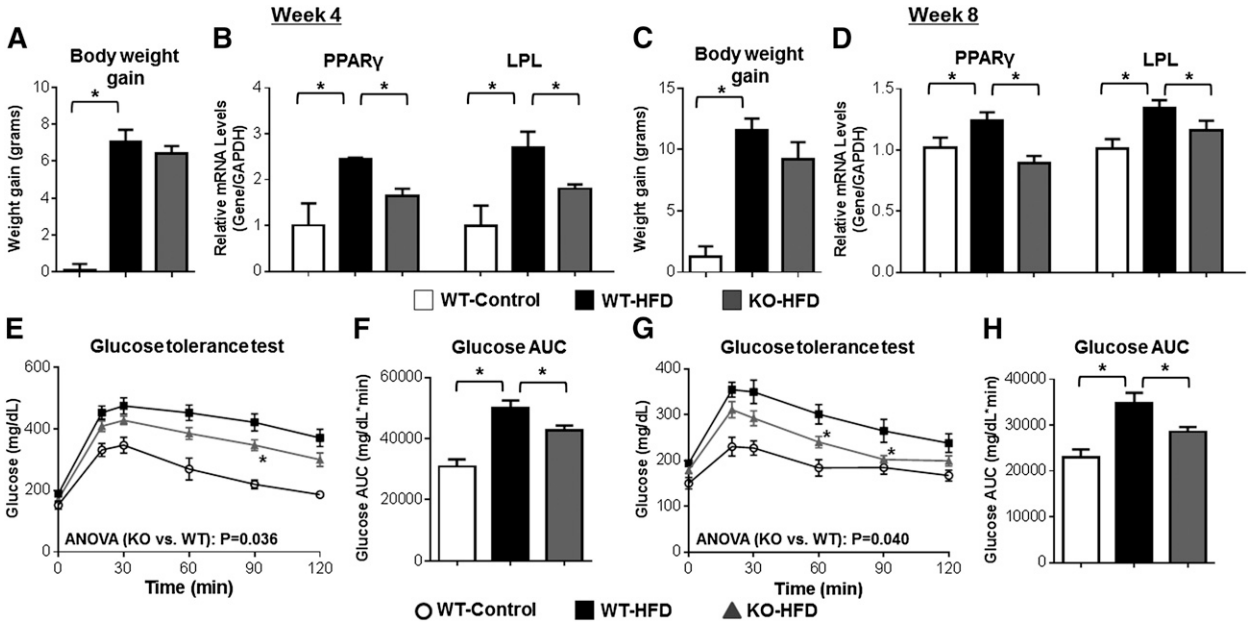

Fig. 9. *Ephx2*$^{-/-}$ mice exhibit attenuated eWAT activation and glucose intolerance following HFD feeding. *Ephx2*$^{-/-}$ and WT mice were fed a HFD (D12079B) or control diet (WT-Control, n = 6; WT-HFD, n = 14; KO-HFD, n = 11) for 4 or 8 weeks. A, C: Total body weight gain from baseline was quantified at 4 weeks (A) and 8 weeks (C). B, D: PPARγ and LPL mRNA levels in eWAT at 4 weeks (n = 3 per group) (B) and 8 weeks (D) (WT-Control, n = 6; WT-HFD, n = 10; KO-HFD, n = 8) were quantified by qRT-PCR, normalized to GAPDH, and expressed relative to the control diet group. E–H: Blood glucose concentrations were quantified at baseline (fasting) and over 120 min following an intraperitoneal glucose tolerance test at 4 weeks (WT-Control, n = 6; WT-HFD, n = 14; KO-HFD, n = 11) (E) and 8 weeks (WT-Control, n = 6; WT-HFD, n = 10; KO-HFD, n = 8) (G). The repeated measures ANOVA *P* value is provided. The corresponding AUC at 4 weeks (F) and 8 weeks (H) was calculated. No significant differences in fasting [week 4 (E), $P = 0.071$); week 8 (G), $P = 0.155$] or fed (week 8, $P = 0.516$) glucose levels between *Ephx2*$^{-/-}$ and WT mice were observed. *$P < 0.05$ versus WT-HFD.

The authors gratefully acknowledge the UNC Department of Cell and Molecular Physiology Histology Core Facility (Kirk McNaughton, director) for their contributions to this work.

REFERENCES

1. Flegal, K. M., M. D. Carroll, B. K. Kit, and C. L. Ogden. 2012. Prevalence of obesity and trends in the distribution of body mass index among US adults, 1999–2010. *JAMA.* **307:** 491–497.
2. Rosen, E. D., C. J. Walkey, P. Puigserver, and B. M. Spiegelman. 2000. Transcriptional regulation of adipogenesis. *Genes Dev.* **14:** 1293–1307.
3. MacDougald, O. A., and M. D. Lane. 1995. Transcriptional regulation of gene expression during adipocyte differentiation. *Annu. Rev. Biochem.* **64:** 345–373.
4. Odegaard, J. I., and A. Chawla. 2013. Pleiotropic actions of insulin resistance and inflammation in metabolic homeostasis. *Science.* **339:** 172–177.
5. Sun, K., C. M. Kusminski, and P. E. Scherer. 2011. Adipose tissue remodeling and obesity. *J. Clin. Invest.* **121:** 2094–2101.
6. Zeldin, D. C. 2001. Epoxygenase pathways of arachidonic acid metabolism. *J. Biol. Chem.* **276:** 36059–36062.
7. Imig, J. D. 2012. Epoxides and soluble epoxide hydrolase in cardiovascular physiology. *Physiol. Rev.* **92:** 101–130.
8. Deng, Y., K. N. Theken, and C. R. Lee. 2010. Cytochrome P450 epoxygenases, soluble epoxide hydrolase, and the regulation of cardiovascular inflammation. *J. Mol. Cell. Cardiol.* **48:** 331–341.
9. Sodhi, K., N. Puri, K. Inoue, J. R. Falck, M. L. Schwartzman, and N. G. Abraham. 2012. EET agonist prevents adiposity and vascular dysfunction in rats fed a high fat diet via a decrease in Bach 1 and an increase in HO-1 levels. *Prostaglandins Other Lipid Mediat.* **98:** 133–142.
10. Bettaieb, A., N. Nagata, D. AbouBechara, S. Chahed, C. Morisseau, B. D. Hammock, and F. G. Haj. 2013. Soluble epoxide hydrolase deficiency or inhibition attenuates diet-induced endoplasmic reticulum stress in liver and adipose tissue. *J. Biol. Chem.* **288:** 14189–14199.
11. Luria, A., A. Bettaieb, Y. Xi, G. J. Shieh, H. C. Liu, H. Inoue, H. J. Tsai, J. D. Imig, F. G. Haj, and B. D. Hammock. 2011. Soluble epoxide hydrolase deficiency alters pancreatic islet size and improves glucose homeostasis in a model of insulin resistance. *Proc. Natl. Acad. Sci. USA.* **108:** 9038–9043.
12. Xu, X., C. X. Zhao, L. Wang, L. Tu, X. Fang, C. Zheng, M. L. Edin, D. C. Zeldin, and D. W. Wang. 2010. Increased CYP2J3 expression reduces insulin resistance in fructose-treated rats and db/db mice. *Diabetes.* **59:** 997–1005.
13. Imig, J. D., A. Elmarakby, K. Nithipatikom, S. Wei, J. H. Capdevila, V. R. Tuniki, B. Sangras, S. Anjaiah, V. L. Manthati, D. Sudarshan Reddy, et al. 2010. Development of epoxyeicosatrienoic acid analogs with in vivo anti-hypertensive actions. *Front. Physiol.* **1:** 157.
14. Khan, M. A., J. Liu, G. Kumar, S. X. Skapek, J. R. Falck, and J. D. Imig. 2013. Novel orally active epoxyeicosatrienoic acid (EET) analogs attenuate cisplatin nephrotoxicity. *FASEB J.* **27:** 2946–2956.
15. Wang, H., Y. Zhao, J. A. Bradbury, J. P. Graves, J. Foley, J. A. Blaisdell, J. A. Goldstein, and D. C. Zeldin. 2004. Cloning, expression, and characterization of three new mouse cytochrome p450 enzymes and partial characterization of their fatty acid oxidation activities. *Mol. Pharmacol.* **65:** 1148–1158.
16. Qu, W., J. A. Bradbury, C. C. Tsao, R. Maronpot, G. J. Harry, C. E. Parker, L. S. Davis, M. D. Breyer, M. P. Waalkes, J. R. Falck, et al. 2001. Cytochrome P450 CYP2J9, a new mouse arachidonic acid omega-1 hydroxylase predominantly expressed in brain. *J. Biol. Chem.* **276:** 25467–25479.
17. Zha, B. S., X. Wan, X. Zhang, W. Zha, J. Zhou, M. Wabitsch, G. Wang, V. Lyall, P. B. Hylemon, and H. Zhou. 2013. HIV protease inhibitors disrupt lipid metabolism by activating endoplasmic reticulum stress and inhibiting autophagy activity in adipocytes. *PLoS ONE.* **8:** e59514.
18. Sinal, C. J., M. Miyata, M. Tohkin, K. Nagata, J. R. Bend, and F. J. Gonzalez. 2000. Targeted disruption of soluble epoxide hydrolase reveals a role in blood pressure regulation. *J. Biol. Chem.* **275:** 40504–40510.
19. Deng, Y., M. L. Edin, K. N. Theken, R. N. Schuck, G. P. Flake, M. A. Kannon, L. M. DeGraff, F. B. Lih, J. Foley, J. A. Bradbury, et al. 2011. Endothelial CYP epoxygenase overexpression and soluble epoxide hydrolase disruption attenuate acute vascular inflammatory responses in mice. *FASEB J.* **25:** 703–713.
20. Edin, M. L., Z. Wang, J. A. Bradbury, J. P. Graves, F. B. Lih, L. M. DeGraff, J. F. Foley, R. Torphy, O. K. Ronnekleiv, K. B. Tomer, et al. 2011. Endothelial expression of human cytochrome P450 epoxygenase CYP2C8 increases susceptibility to ischemia-reperfusion injury in isolated mouse heart. *FASEB J.* **25:** 3436–3447.
21. Theken, K. N., Y. Deng, R. N. Schuck, A. Oni-Orisan, T. M. Miller, M. A. Kannon, S. M. Poloyac, and C. R. Lee. 2012. Enalapril reverses high-fat diet-induced alterations in cytochrome P450-mediated eicosanoid metabolism. *Am. J. Physiol. Endocrinol. Metab.* **302:** E500–E509.
22. Theken, K. N., Y. Deng, M. A. Kannon, T. M. Miller, S. M. Poloyac, and C. R. Lee. 2011. Activation of the acute inflammatory response alters cytochrome p450 expression and eicosanoid metabolism. *Drug Metab. Dispos.* **39:** 22–29.
23. Livak, K. J., and T. D. Schmittgen. 2001. Analysis of relative gene expression data using real-time quantitative PCR and the 2(-Delta Delta C(T)) method. *Methods.* **25:** 402–408.
24. Zha, W., G. Liang, J. Xiao, E. J. Studer, P. B. Hylemon, W. M. Pandak, Jr., G. Wang, X. Li, and H. Zhou. 2010. Berberine inhibits HIV protease inhibitor-induced inflammatory response by modulating ER stress signaling pathways in murine macrophages. *PLoS ONE.* **5:** e9069.
25. Morisseau, C., and B. D. Hammock. 2007. Measurement of soluble epoxide hydrolase (sEH) activity. *Curr. Protoc. Toxicol.* **33:** 4.23.1–4.23.18.
26. Theken, K. N., R. N. Schuck, M. L. Edin, B. Tran, K. Ellis, A. Bass, F. B. Lih, K. B. Tomer, S. M. Poloyac, M. C. Wu, et al. 2012. Evaluation of cytochrome P450-derived eicosanoids in humans with stable atherosclerotic cardiovascular disease. *Atherosclerosis.* **222:** 530–536.
27. Osman, O. S., J. L. Selway, M. A. Kepczynska, C. J. Stocker, J. F. O'Dowd, M. A. Cawthorne, J. R. Arch, S. Jassim, and K. Langlands. 2013. A novel automated image analysis method for accurate adipocyte quantification. *Adipocyte.* **2:** 160–164.
28. Mathes, W. F., D. L. Aylor, D. R. Miller, G. A. Churchill, E. J. Chesler, F. P. de Villena, D. W. Threadgill, and D. Pomp. 2011. Architecture of energy balance traits in emerging lines of the Collaborative Cross. *Am. J. Physiol. Endocrinol. Metab.* **300:** E1124–E1134.
29. Ayala, J. E., V. T. Samuel, G. J. Morton, S. Obici, C. M. Croniger, G. I. Shulman, D. H. Wasserman, and O. P. McGuinness. 2010. Standard operating procedures for describing and performing metabolic tests of glucose homeostasis in mice. *Dis. Model. Mech.* **3:** 525–534.
30. Xia, J., R. Mandal, I. V. Sinelnikov, D. Broadhurst, and D. S. Wishart. 2012. MetaboAnalyst 2.0–a comprehensive server for metabolomic data analysis. *Nucleic Acids Res.* **40:** W127–W133.
31. Zhao, X., A. Dey, O. P. Romanko, D. W. Stepp, M. H. Wang, Y. Zhou, L. Jin, J. S. Pollock, R. C. Webb, and J. D. Imig. 2005. Decreased epoxygenase and increased epoxide hydrolase expression in the mesenteric artery of obese Zucker rats. *Am. J. Physiol. Regul. Integr. Comp. Physiol.* **288:** R188–R196.
32. Mothe-Satney, I., C. Filloux, H. Amghar, C. Pons, V. Bourlier, J. Galitzky, P. A. Grimaldi, C. C. Feral, A. Bouloumie, E. Van Obberghen, et al. 2012. Adipocytes secrete leukotrienes: contribution to obesity-associated inflammation and insulin resistance in mice. *Diabetes.* **61:** 2311–2319.
33. Ghoshal, S., D. B. Trivedi, G. A. Graf, and C. D. Loftin. 2011. Cyclooxygenase-2 deficiency attenuates adipose tissue differentiation and inflammation in mice. *J. Biol. Chem.* **286:** 889–898.
34. Vanella, L., D. H. Kim, K. Sodhi, I. Barbagallo, A. P. Burgess, J. R. Falck, M. L. Schwartzman, and N. G. Abraham. 2011. Crosstalk between EET and HO-1 downregulates Bach1 and adipogenic marker expression in mesenchymal stem cell derived adipocytes. *Prostaglandins Other Lipid Mediat.* **96:** 54–62.
35. De Taeye, B. M., C. Morisseau, J. Coyle, J. W. Covington, A. Luria, J. Yang, S. B. Murphy, D. B. Friedman, B. B. Hammock, and D. E. Vaughan. 2010. Expression and regulation of soluble epoxide hydrolase in adipose tissue. *Obesity (Silver Spring).* **18:** 489–498.
36. Kim, D. H., L. Vanella, K. Inoue, A. Burgess, K. Gotlinger, V. L. Manthati, S. R. Koduru, D. C. Zeldin, J. R. Falck, M. L. Schwartzman, et al. 2010. Epoxyeicosatrienoic acid agonist regulates human mesenchymal stem cell-derived adipocytes through activation of HO-1-pAKT signaling and a decrease in PPARγ. *Stem Cells Dev.* **19:** 1863–1873.

37. Burgess, A. P., L. Vanella, L. Bellner, K. Gotlinger, J. R. Falck, N. G. Abraham, M. L. Schwartzman, and A. Kappas. 2012. Heme oxygenase (HO-1) rescue of adipocyte dysfunction in HO-2 deficient mice via recruitment of epoxyeicosatrienoic acids (EETs) and adiponectin. *Cell. Physiol. Biochem.* **29:** 99–110.
38. Madsen, L., R. K. Petersen, M. B. Sorensen, C. Jorgensen, P. Hallenborg, L. Pridal, J. Fleckner, E. Z. Amri, P. Krieg, G. Furstenberger, et al. 2003. Adipocyte differentiation of 3T3–L1 preadipocytes is dependent on lipoxygenase activity during the initial stages of the differentiation process. *Biochem. J.* **375:** 539–549.
39. Wang, M., J. J. Wang, J. Li, K. Park, X. Qian, J. X. Ma, and S. X. Zhang. 2009. Pigment epithelium-derived factor suppresses adipogenesis via inhibition of the MAPK/ERK pathway in 3T3–L1 preadipocytes. *Am. J. Physiol. Endocrinol. Metab.* **297:** E1378–E1387.
40. Li, F., D. Wang, Y. Zhou, B. Zhou, Y. Yang, H. Chen, and J. Song. 2008. Protein kinase A suppresses the differentiation of 3T3–L1 preadipocytes. *Cell Res.* **18:** 311–323.
41. Dagon, Y., Y. Avraham, and E. M. Berry. 2006. AMPK activation regulates apoptosis, adipogenesis, and lipolysis by eIF2alpha in adipocytes. *Biochem. Biophys. Res. Commun.* **340:** 43–47.
42. Yang, S., L. Lin, J. X. Chen, C. R. Lee, J. M. Seubert, Y. Wang, H. Wang, Z. R. Chao, D. D. Tao, J. P. Gong, et al. 2007. Cytochrome P-450 epoxygenases protect endothelial cells from apoptosis induced by tumor necrosis factor-alpha via MAPK and PI3K/Akt signaling pathways. *Am. J. Physiol. Heart Circ. Physiol.* **293:** H142–H151.
43. Carroll, M. A., A. B. Doumad, J. Li, M. K. Cheng, J. R. Falck, and J. C. McGiff. 2006. Adenosine2A receptor vasodilation of rat preglomerular microvessels is mediated by EETs that activate the cAMP/PKA pathway. *Am. J. Physiol. Renal Physiol.* **291:** F155–F161.
44. Cannon, B., and J. Nedergaard. 2004. Brown adipose tissue: function and physiological significance. *Physiol. Rev.* **84:** 277–359.
45. Spiegelman, B. M. 2013. Banting Lecture 2012: Regulation of adipogenesis: toward new therapeutics for metabolic disease. *Diabetes.* **62:** 1774–1782.
46. Wang, Q. A., C. Tao, R. K. Gupta, and P. E. Scherer. 2013. Tracking adipogenesis during white adipose tissue development, expansion and regeneration. *Nat. Med.* **19:** 1338–1344.
47. Yamauchi, T., H. Waki, J. Kamon, K. Murakami, K. Motojima, K. Komeda, H. Miki, N. Kubota, Y. Terauchi, A. Tsuchida, et al. 2001. Inhibition of RXR and PPARgamma ameliorates diet-induced obesity and type 2 diabetes. *J. Clin. Invest.* **108:** 1001–1013.
48. Rieusset, J., F. Touri, L. Michalik, P. Escher, B. Desvergne, E. Niesor, and W. Wahli. 2002. A new selective peroxisome proliferator-activated receptor gamma antagonist with antiobesity and antidiabetic activity. *Mol. Endocrinol.* **16:** 2628–2644.
49. Lee, Y. S., P. Li, J. Y. Huh, I. J. Hwang, M. Lu, J. I. Kim, M. Ham, S. Talukdar, A. Chen, W. J. Lu, et al. 2011. Inflammation is necessary for long-term but not short-term high-fat diet-induced insulin resistance. *Diabetes.* **60:** 2474–2483.